NJC

RSC Publishing

PAPER

View Article Online
View Journal | View Issue

Cite this: *New J. Chem.*, 2013, **37**, 2110

Equilibrium structure and dynamics of organic crystals by Monte Carlo simulation: critical assessment of force fields and comparison with static packing analysis†

Angelo Gavezzotti*

The atom–atom intermolecular force field AA-CLP with subdivision of interaction energies into Coulomb-polarization, dispersion (London) and repulsion (Pauli) terms is applied to the Monte Carlo simulation of 63 organic crystals taken from the literature to cover the most common functionalities of organic and biological chemistry. Non-rigid molecules are treated as ensembles of rigid fragments connected by torsional degrees of freedom, for which *ad hoc* potentials are obtained from MP2-631G** calculations. The performance of the method and force field is assessed by comparison with experimental structures at 100 and 300 K. Molecular orientation, cell dimensions and sublimation energies are well reproduced, with some exceptions for fluorinated and nitro compounds. Simulated density and energy changes with temperature reproduce experimental observations. Calculated radial density functions and correlation functions reveal details of material behaviour at the atomic level, including librational amplitudes. Dynamic phenomena like methyl group rotations or rotational diffusion in the classic case of the benzene derivatives and adamantane are described in a satisfactory manner. Competition between intra- and intermolecular factors in biphenyl and other double-ring compounds is accurately described. Use of dynamic or Monte Carlo simulation gives a realistic picture of crystal structure and bonding, which often contrasts with simplistic views postulated on the basis of averaged atomic positions and static packing diagrams, as produced in typical single-crystal X-ray diffraction experiments.

Received (in Montpellier, France) 15th February 2013,
Accepted 9th April 2013

DOI: 10.1039/c3nj00181d

www.rsc.org/njc

Introduction

Atom–atom force fields are computational devices that allow extensive and reasonably inexpensive simulation of organic condensed phases. In a static approach, the energies of single points in crystal phase space are evaluated and are compared among themselves to find energy minima, or are compared with experimental thermochemical data, typically sublimation enthalpies, providing the main pathway for the optimization of potential parameters. Much more rewarding is the exploration of phase space *via* molecular dynamics (MD) or Monte Carlo (MC) methods, which allow the reproduction or prediction of thermophysical quantities like equilibrium densities and radial distribution functions in crystals and in liquids, the study of dynamic diffusion phenomena, and, at least in principle, may open the way to the simulation of phase transitions. For crystals, for example, MD has been extensively used[1–3] and its performance has been analyzed with comparisons of force field performance.[4] MC is routinely used in the optimization of the fit between experiment and calculation for the solution of powder crystal studies,[5] and in the simulation of crystal growth;[6,7] it is a staple of the molecular simulation of liquid crystals.[8] Its reaction-ensemble variant has been used to simulate polymorphic phase behaviour.[9] Details of crystal melting have been explored by MD,[10,11] while crystal assembling has been tentatively studied by biased MC methods[12] and by MD.[13] Crystal structure prediction, the most ambitious task of molecular simulation of solids, has been tackled by MC[14,15] and MD.[16–19a] The study of crystal growth by MD is becoming feasible.[19b] The above list of citations is of course more indicative than exhaustive.

An intermolecular force field including separate contributions from Coulombic, polarization, and London–Pauli dispersion and repulsion factors (the CLP force field) has been presented[20] for compounds including H, C, N, O, F and Cl atoms. The method requires the input of a few atomic properties, like electronegativities

Department of Chemistry, University of Milano, via Venezian 21, 20133 Milano, Italy. E-mail: angelo.gavezzotti@unimi.it

† Electronic supplementary information (ESI) available: Details of force fields, molecular geometries, and extensive results. Tables S1–S5. Fig. S1–S16. See DOI: 10.1039/c3nj00181d

or ionization potentials, and a number of *ad hoc* modulation parameters. Atom–atom interaction potentials are established for each atom pair in a given molecule, rather than for all atoms of a given atomic species, on the basis of an estimate of the electron charge excess or depletion in each atomic basin. The AA-CLP construct is but a broad interpretation of physical realism, but it is extremely convenient in terms of man- and computer-time, and it has been shown, after careful parameterization, to reproduce the (static) sublimation enthalpies of about 150 crystals and the physical properties of a variety of organic solvents in Monte Carlo treatment.[20] The subdivision of total energies into Coulombic and dispersion–repulsion provides some chemical understanding in addition to bare energy numbers.

The present contribution reports the systematic application of the complete force-field plus Monte Carlo scheme to 63 organic crystals, studying their equilibrium properties and the representation of dynamic properties like methyl librations and rotational diffusion. The good performance and the limitations of atom–atom formulations are discussed also in view of their use for the study of liquid–solid phase transitions.

Computational methods

The relevant algebra, while more details on the lines of reasoning that led to the formulation of the AA-CLP force field, can be found in the original paper.[20] For a given i–j atom pair the Coulomb–London–Pauli (CLP) interaction function has terms for Coulombic, polarization, dispersion and repulsion:

$$E_{i,j} = 1/(4\pi\varepsilon^{\circ})\,(q_i q_j)R_{i,j}^{-1} - F_P P_{i,j} R_{i,j}^{-4} - F_D D_{i,j} R_{i,j}^{-6} + F_R T_{i,j} R_{i,j}^{-12} \quad (1)$$

where $R_{i,j}$ is an internuclear distance, and $q_i = F_Q q_i^{\circ}$ is the rescaled net charge population on atom i. F_Q, F_P, F_D and F_R are empirical scaling parameters, while P, D and T are coefficients calculated on the basis of the local environment of an atom in a given molecule. The scaling factors in eqn (1) were kept at the previously[20] optimized values ($F_Q = 0.41$, $F_P = 235$, $F_D = 650$, $F_R = 77\,000$). Details are collected in Table S1 (ESI†).

Crystal structures were retrieved from the Cambridge Structural Database[21] with the usual[22] renormalization of hydrogen-atom positions. A selection of substituted benzenes (Table 1) was included as a sample for the study of substitution patterns on crystal structure. Crystal structures of linear-chain alkanes R–$(CH_2)_n$–R were included for R = methyl (n = 4, 5, 6), R = OH and COOH (n = 4, 5). Scheme 1 shows non-obvious structural formulae. The total number of crystal structures considered is 63, including different chemical classes, rigid and conformationally flexible molecular frames, as well as different crystal systems and space groups. Details are collected in Table S2 (ESI†).

The total Monte Carlo configurational energy is a sum of intramolecular and intermolecular terms. In general:

$$E(\text{tot}) = \Sigma f(\tau, \text{tors}) + \Sigma f(\text{bend}) + \Sigma U(\text{interm}) \quad (2)$$

where each summation runs over the appropriate degrees of freedom. For the torsional terms, $f(\tau)$, the energy profiles are calculated by *ab initio* MP2-6-31G** and fitted in cosine or polynomial forms.

Table 1 Crystal structures of substituted benzenes. Melting temperatures are given for low-melting (<300 K) crystals

Compound	Description	T (melt)	CSD refcode[a]
Benzene	X = H	279	benzen07
Nitrobenzene	X = NO_2	279	nitrbe01*
Benzoic acid	X = COOH		benzac07
Benzamide	X = $CONH_2$		bzamid01
Acetanilide	X = $NHC(O)CH_3$		acanil01
Biphenyl	X = Ph		biphen04
1,2-Di(X)benzene	X = F	239	facfoe**
	X = Cl	256	Abumit
	X = CN		yuypud01
	Naphthalene		naphta10
1,3-Di(X)benzene	X = CH_3	226	zzzspy01
	X = NO_2		dnbenz14*
1,4-Di(X)benzene	X = CH_3		zzzity01
	X = F	260	facgev
	X = Cl		dclben01
	X = Cl		dclben02
	X = NO_2		dnitbz11*
	X = CN		tepnit11
	X = COOH		tephth06
	Benzoquinone		bnzqui03*
1,4-(XY)benzene	X = OH, Y = CHO		phbald11
	X = OH, Y = CH_2OH		fovqox
	X = CH_3, Y = CCH	unav	ayojed
1,2,3-Tri(X)benzene	X = F	>235	pugdeb
1,3,5-Tri(X)benzene	X = F	269	pvvawa01**
	X = Cl		tchlbz03
1,2,4,5-Tetra(X)benzene	X = F	278	facjau
Hexa(X)benzene	X = Cl		hclbnz11

[a] No stars, simulation OK; one star, simulation with imperfect convergence; two stars, simulation bad, compound excluded from the dataset.

Bending energy profiles calculated *ab initio* and bending terms in a harmonic form are included only for COH angles in carboxylic acids and alcohols, and for CNH angles in amides. The intermolecular potential is the CLP field of eqn (1). Details of the force field for each molecule are in Table S3 (ESI†).

For the simulation of a crystal structure (in general) an oblique simulation box is prepared by repeating the unit cell to box dimensions of 30–40 Å, preserving cell angles. The number of molecules in each box ranged from 200 to 500 depending on molecular size. Molecular positions are specified by three translational center-of-mass and three rotational rigid-body parameters. Conformation for non-rigid molecules is specified by the values of internal torsional and bending parameters. Periodic boundary conditions apply with pressure control by the isothermal–isobaric ensemble procedure.[23] Changes in cell dimensions (all six together) are attempted every 900, 1100 or 1300 steps for triclinic, monoclinic and orthorhombic systems, respectively (angles equal to 90° by crystal system symmetry are also allowed to vary). Cell changes are implemented by de-orthogonalizing in the old metrics and re-orthogonalizing in the new metrics. Acceptance ratios were 50–70% for both cell variations and molecular moves. Run lengths were 5 Msteps (1 Mstep = 1 megastep = 1 000 000 MC steps). Pressure was set at 1 atm and temperature at 100 or 300 K. For more details on simulation conditions see Table S4 (ESI†).

Final simulation values for cell parameters and lattice energies (Table S5, ESI†) were determined by averaging trajectory data in the last 3 Msteps (production) with estimated rmsds from the

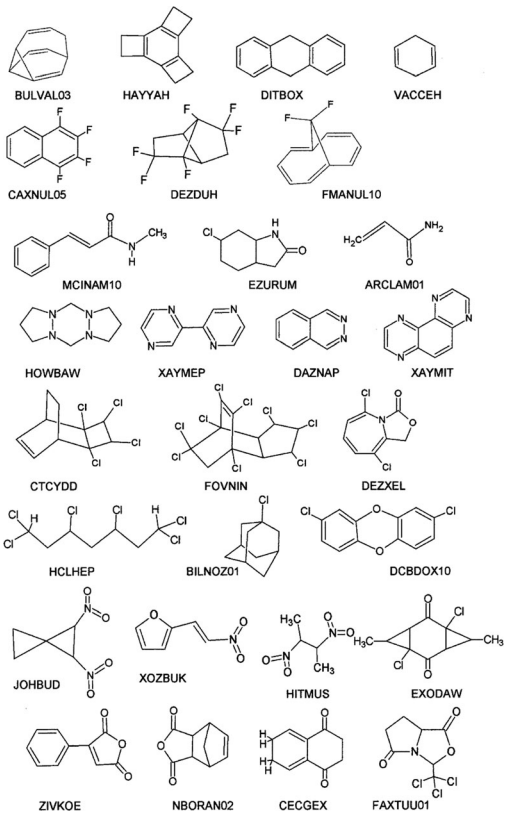

Scheme 1 Formulae for compounds not obvious by nomenclature. The CSD refcode[22] is shown under each diagram. VACCEH is the only low-melting crystal.

average. Radial distribution functions (RDFs) and angular and rotational correlation functions were calculated in the usual way:[20] for RDF's, either on the last frame of the simulation – an instant snapshot of the system – or on frames generated by averaging the last 10 frames, or 1 Mstep, of each simulation run; for correlation functions, using the crystal frame as reference.

The simulations presented here require only ordinary desktop–laptop computers under MS-Windows, with typical running times of less than one hour per Mstep. For more details see *CLPmanual.doc* available at http://users.unimi.it/gavezzot in the CLP computer program package. The set of programs, entirely developed in-house, includes modules for static atom–atom crystal calculation and energy optimization, modules for preparation of liquid and crystal computational boxes, for Monte Carlo runs (for crystals, limited to triclinic, monoclinic or orthorhombic symmetry and one or two molecules in the asymmetric unit), and for trajectory analysis. Source codes with examples are available for download from the same site. Written notice to the author at his e-mail address is kindly requested.

Results and discussion

Equilibrium structures

Ideally, a simulation with a perfect potential and a perfect temperature–pressure control mechanism (a) should not change the observed cell parameters or the starting lattice energies, and (b) should not change the molecular orientation and the position in the cell, or the molecular conformation. A convergent simulation (one that has reached a plateau of Boltzmann equilibrium) should have small rmsds from average properties in the production stage. Four crystals: 1,2-difluoro- and 1,3,5-trifluorobenzene, 1,2,3,4-tetrafluoronaphthalene (CAXNUL05) and the hexachloroheptane (HCLHEP) were completely outside the above limits, and were excluded from further analysis, which then concerns only 59 crystals.

In principle, comparison between the equilibrated MC structure and the structure resulting from pure lattice energy minimization should deconvolute the effects of force field shortcomings (apparent in the latter) from the effects of the dynamic treatment (apparent in both). In practice however temperature-less energy minimizations always lead to a structure distortion, being formally a prediction of the structure at zero temperature; detailed analysis of each case is therefore scarcely rewarding. Interestingly however, minimization for the trifluorobenzene and the tetrafluoronaphthalene led to large displacements, in agreement with the MC simulation, while minimization for the other two compounds was featureless. We hesitate to draw further conclusions on these cases. Lattice energy minimizations for the other compounds gave results in broad agreement with the pattern of the MC simulations.

Fig. 1 shows that the simulations at 100 K mostly produce an increase in density, in part due to the lowering of the temperature from that of the X-ray determination, but in part due to

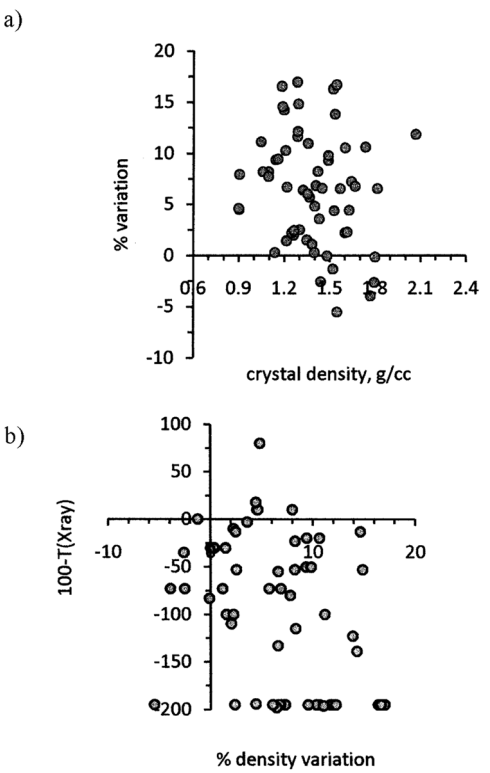

Fig. 1 (a) Percent change in density in the simulations at 100 K. (b) Comparison with the formal temperature change from the temperature of the X-ray experiment. The lower-right sector of the graph corresponds to contraction on cooling. Sample of 59 (63 − 4 excluded as wrong) crystal structures.

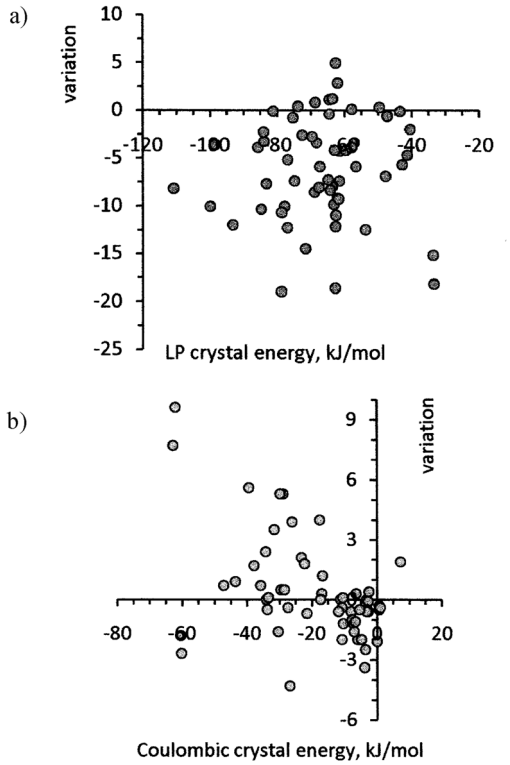

Fig. 2 (a) Changes in polarization–dispersion–repulsion (LP) energy in the simulations at 100 K. (b) The same for Coulombic energies. kJ mol^{-1} units.

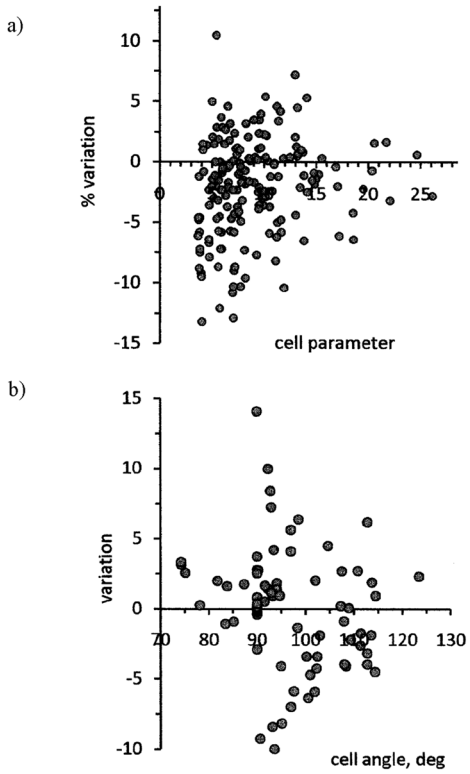

Fig. 3 Percent changes in cell parameters (a, Å) and change in cell angles (b, degrees) in the simulations at 100 K.

poor performance of the potentials (convergence is assured by rmsds never exceeding 0.004 g cm^{-3}, Fig. S1, ESI†). Correspondingly, total lattice energies become more stabilizing (Fig. S2a, ESI†) but also converge properly (Fig. S2b, ESI†), rmsds never exceeding 0.25 kJ mol^{-1}. Fig. 2 shows that the stabilization is mostly due to an increase in dispersion energies, while Coulombic energies behave erratically.

In the atom–atom point-charge method, dispersion energies are similar to those coming from more accurate methods, while Coulombic energies are underestimated due to the lack of penetration energy – the stabilizing energy that comes from interpenetration of negatively charged outer electron clouds to reach the nuclei of neighbouring molecules. This contribution is reproduced only in delocalized descriptions such as the PIXEL approach.[24] Table 2 shows some comparisons. Such a poor description of Coulombic forces is intrinsic to the point-charge method; the discussion in the next paragraphs demonstrates however that this shortcoming is relevant for second-row elements and saturated alkanes, but in general does not hamper an equilibrium simulation for organic crystals, where dispersion often dominates. Anyway, it is important to be aware of those inadequacies, especially when discussing relative energies of polymorphs or the energy ranking of predicted crystal structures.

Table 2 Calculated Coulombic, polarization, dispersion, repulsion and total lattice energies[a]

Crystal	E_{coul}	E_{pol}	E_{disp}	E_{rep}	E_{tot}
C_6Cl_6	−23	−12	−148	91	−94
	+7	−4	−135	39	−94
1,3,5-Trichlorobenzene	−20	−8	−100	56	−72
	+1.0	−8	−101	31	−77
n-Hexane	−11	−5	−77	45	−48
	+1	−21	−63	23	−59

[a] First row: PIXEL, second row: AA-CLP energies (kJ mol^{-1}).

Fig. 3 shows the landscape of variation of cell parameters in the simulations at 100 K. A change of 5% or 5° is considered almost within the noise level and hence tolerable. Fig. S3a and b (ESI†) show the corresponding convergence tests, in which cell edge rmsds never exceed 0.04 Å and cell angle rmsds never exceed 0.5°. Outliers are nitrobenzene, 1,4-dinitrobenzene, and benzoquinone. There is a moderate, obvious trend to increasing density with a decrease in cell parameters, although in some cases cell edges change in opposite directions, representing a distortion of the crystal structure at constant density and lattice energy. A positive result, for which there is no immediate explanation, is that angles equal to 90° in orthorhombic or monoclinic systems almost never change by more than 1°. The agreement between calculated lattice energies and experimental sublimation enthalpies[25] can be considered excellent (Fig. S4, ESI;† see also ref. 20).

Intramolecular energies seem to be scarcely relevant in the simulation. Of the 29 flexible molecules considered only 5 exhibit a substantial change in this contribution, corresponding to a conformational rearrangement (Fig. S5, ESI†). For glutaric and terephthalic acid, the C–O–H angles change from 113° to 105°, for acetanilide, there is an increase of the

ring-substituent torsion angle from 18° to a 30–50°distribution (the torsional energy profile may be too steep at low τ). For MCINAM and EXODAW (see Scheme 1) the stabilization concerns a reorientation of the methyl groups; methyl group reorientation is the subject of one of the forthcoming sections in this paper.

Temperature dependence

5 Mstep crystal structure simulations were carried out at 300 K starting from the final result of the simulations at 100 K. Some of the compounds considered melt at some 20–30 K below 300 K (Table 1), but the simulation of what would be formally a liquid helps in highlighting and discriminating rotational behaviour. For the *n*-alkanes and the two aliphatic alcohols, the simulation at a temperature of 60–100 K higher than the melting temperature allows a clearer estimation of the molecular diffusion effects typical of these crystals.

Density and energy changes from the original static X-ray structure are shown in Fig. 4 and 5, respectively. Compounds that are (barely) liquid at 300 K obviously show larger changes. Cell edge and cell angle changes are shown in Fig. S6 (ESI†), and are all positive (edges) and very small (angles). The average density change of 4% over 200 K coincides with the average experimental thermal expansion coefficient[26a] for organic crystals, $1/V(\mathrm{d}V/\mathrm{d}T) = 2 \times 10^{-4}\ \mathrm{K}^{-1}$. The rise in energy of 5–10 kJ mol^{-1} over 200 K agrees in order of magnitude with the average experimental C_p of organic crystals, $\approx$100 J K^{-1} mol^{-1},[26b] recalling that our calculated value is only the intermolecular part of C_p. These results lend in general further confidence to the method and the force field, although a detailed comparison of calculated and experimental values for single cases would be problematic.

General structural features

For compounds containing flat aromatic systems, a tolerable defect is a tendency to increase the crystal density and to decrease interplanar angles to a more parallel stacking of aromatic rings, as evidenced by shifts of 0.2–0.3 Å in the peaks of center-of-mass RDF's (Fig. S7, ESI†). The oscillation amplitude of the interplanar angles, from the snapshot in the last frame of the simulation, is ~10° at room *T* and decreases to ~5 at 100 K

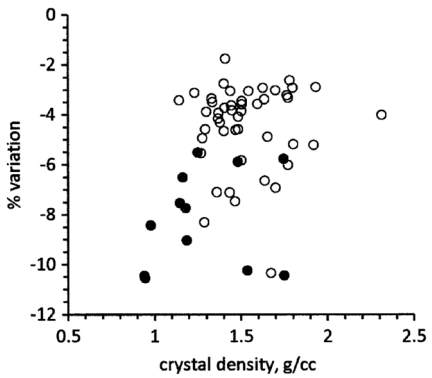

Fig. 4 Percent change in density on going from 100 to 300 K. Shaded circles: compounds that are liquid at 300 K.

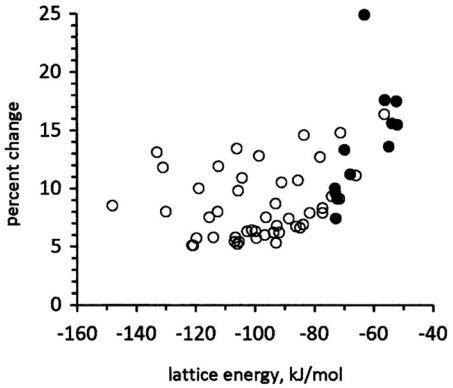

Fig. 5 Percent change in lattice energy (total configurational energy) on going from 100 to 300 K. Shaded circles: compounds that are liquid at 300 K.

(see Fig. S8, ESI†). For these typical cases C···C radial distribution function shows pronounced tails down to *R* = 3.2 Å (Fig. S9, ESI†). Thus, according to the simulations, an instantaneous C···C separation of 10% less than the sum of atomic radii is a normal event in a molecular crystal at room temperature.

Of the four simulation failures, three involve fluorine derivatives, having large structure rearrangements at little energy expense, as if suggesting a phase transition to a different polymorph. No systematic reason has been found for these results: for example, 1,2-difluorobenzene is a failure but the 1,4-isomer is ok; 1,3,5-trifluorobenzene is a failure but the 1,2,3-isomer is ok. After 5 Msteps the crystal of tetrafluoronaphthalene (CAXNUL, Scheme 1) is still drifting to large structural rearrangement. The F···F RDF has a single broad plateau from 3.2 to 6 Å and beyond (Fig. S10, ESI†). This behavior defines interpretation. Aliphatic fluoro derivatives show less anomaly than aromatic derivatives in the simulations. Either aromatic fluorine crystals include some subtle energetic modulation that escapes the rudimentary atom–atom formulation, or these structures are indeed prone to stacking slippage or other forms of dynamic rearrangement, roughly speaking, in terms of the lack of internal friction/cohesion (see also the section on molecular rotations), a counterpart of the well known lack of adhesion of fluorinated materials. Anyway, fluorine confirms here its odd-man-out nature.[27]

The MC-CLP description of aromatic chlorobenzenes is satisfactory. Crystal structures and sublimation enthalpies are well reproduced. The simulations predict an increase in density (an average of 7.8% for the five crystals), common to all aromatic planar compounds. In the equilibrated polychlorobenzene structures, Cl···Cl radial density functions show broad bands with Cl···Cl contacts in the 3.2–4.2 Å range (Fig. S11, ESI†), reflecting on the lower side transient compression of the intermolecular Cl···Cl separation, on the upper side the wide variability and non-specificity of such contacts, once invoked as factors of crystal stability. The two considered polymorphs of 1,4-dichlorobenzene show a peak in the Cl···Cl RDF at 3.6 Å (Fig. S11, ESI†), failing to reproduce the difference between the 3.8 Å peak of the monoclinic polymorph (T-shaped C–Cl···Cl–C contacts) and the 3.4 Å peak of the triclinic polymorph (linear

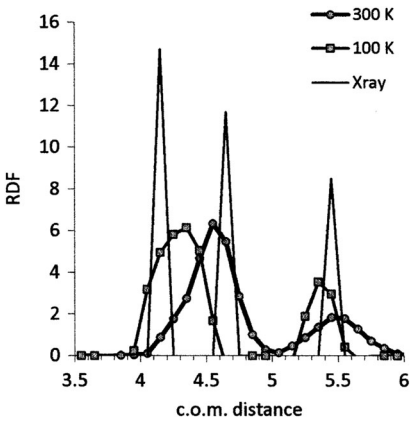

Fig. 6 Radial distribution function of the center of mass distance in the experimental and simulated crystal structure of *n*-hexane.

C–Cl···Cl–C contacts). Presumably, atom–atom isotropic potentials with a localized charge obviously fail to reproduce such a fine directional detail. The crystal structures of aliphatic chloro compounds are better reproduced in the simulations, with density increases of just 3.5%.

Alkane crystals with odd or even C-atom number behave in the same way in MC simulations. Heats of sublimation are well reproduced and distortions in cell dimensions are minor. The molecular conformation in the crystal is invariably all-*trans* and staggered. The first two peaks in the centers-of-mass RDF of the experimental structures (Fig. 6), for the two cell edges perpendicular to the chain elongation, are at 4.1 and 4.7 Å; in the simulation, these two peaks merge into a single peak at 4.4 Å. This is in part due to a roughness of the force field, the Coulombic energy being intrinsically badly represented in the absence of penetration energies (Table 2), and in part due to the effect of rotational molecular displacement. The large shift and increase in width of the first center-of-mass RDF on going from 100 K to room temperature (Fig. 6) reflect the premelting behavior of the crystal. These are examples of the different impression that one gathers from static and from dynamic analysis.

Hydrogen bonding and C–H···O contacts

The key parameters in the description of hydrogen bonding are the H···acceptor distance and its oscillation limits (Table 3; RDF details are given in Fig. S12, ESI†), and the torsional angle over the O═C–O–H, O═C–N–H or C–C–O–H group for acids, amides and alcohols, respectively. For carboxylic acids the predicted average H-bonding distance is slightly longer than experiment, and the oscillation shows but a hint of anharmonicity. Aromatic acids exhibit a stronger O–H···O hydrogen bond; terephthalic acid has the shortest distance of 1.77 Å, and the smallest amplitude of ±0.20 Å. For amides the result is quite similar, with an average predicted N–H···O distance slightly longer than experiment, and a slightly larger stretching amplitude as appropriate to a weaker bond. Amides also show a more marked anharmonicity and a larger fluctuation of the torsion angle. The O–H···O hydrogen bonding distance in alcohols is perfectly reproduced in the MC simulation. The distributions of H–O–C–C torsion

Table 3 Average results of MC simulations at room temperature against experimental static values for some hydrogen-bonding intermolecular interactions (Å units)

Interaction type	Exptl (X-ray)	Equilibrium H-bond distance[a]	Range[b]	τ Range[c]
O–H···O acids	1.65	1.77 to 1.80 arom 1.80 to 1.83 aliph	−0.13; +0.18 −0.20; +0.32	15
N–H···O amides	1.95	2.05 to 2.15	−0.23: +0.25 (+0.45 aliph)	20 to 40°
O–H···O alcohol	1.75	1.72 to 1.77	−0.22; +0.26	≈20°

[a] Distance at the first peak in the RDF of the last frame of the simulation. [b] Width of the first peak: left and right span from the maximum in the RDF. [c] Spread of the HCCO, HNCO or HOCC torsion angle distribution from planarity in acids and amides; from crystal equilibrium in alcohols.

angles for the two aliphatic alcohols, simulated at 300 K, higher than their melting points, show occasional 40–50° jumps, a pre-melting, hydrogen-bond breaking process. In 1,4-butanediol (QATTIO) the two OH's are not equal by symmetry. The torsion angles on the two OH functions are identical in the static picture (τ = 173°), but differ in the dynamics at 300 K, one of the two being prone to 30° jumps due to a weaker intermolecular constraint. These are more examples of information that could never have been gained by inspection of the static crystal packing.

The crystal structures of compounds with C, H and O atoms only, without classical OH···O hydrogen bonds are very well reproduced by the MC simulation, with the exception of benzoquinone, whose simulation is scarcely convergent. In what concerns the critical interactions between positively charged terminals (CH) and prospective proton acceptors (especially carbonyl oxygens), Fig. 7 shows some typical results. Unexpectedly, the aliphatic CH groups form shorter contacts with carbonyl oxygens than aromatic CH groups, in spite of the lesser acidity. Moreover, the separate peaks observed in the static representation of the crystal in the 2.5–3.5 Å region are in fact broad peaks in the corresponding RDF's, and merge into a single dome in the instantaneous representation of the single-frame snapshot

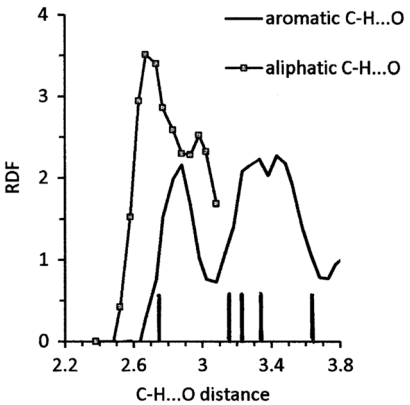

Fig. 7 Radial distribution functions of C–H···O contacts in norbornene anhydride (NBORAN; average over the last 10 frames at 300 K). Vertical bars mark the distances in the experimental crystal structure. In the last frame the dip in the aromatic RDF disappears and all peaks merge into a single dome.

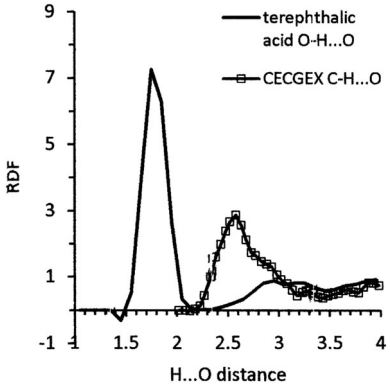

Fig. 8 Comparison of radial distribution function of CH···O and O–H···O contacts. CECGEX: see molecular structure in Scheme 1.

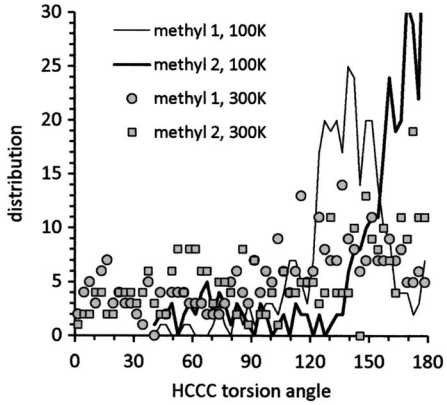

Fig. 9 Histogram of HCCC torsion angles in the final frame of the MC simulation of 1,3-dimethylbenzene. One H-atom is taken as arbitrary reference so that each quoted angle τ has two equivalents at $\tau + 120^\circ$ and $\tau + 240^\circ$ (*mod*. 360).

(Fig. S13, ESI†). When studying crystal structures in terms of atom–atom separations, one should keep in mind that thermal libration makes so that what appear as distinct interactions in a static view, actually live in largely overlapping energy wells. For example, upon comparing the results for the transient behaviour of O–H···O and C–H···O interactions (Fig. 8), one has a clearer picture of the substantial difference between the two effects. The C–H···O interaction, spanning a 2.4 to 3.4 Å distance range, is better described as a transient approach preference due to Coulombic interaction, rather than as a bond in a proper chemical sense. Within a range of 1 Å such a preference can be satisfied in many different ways in a crystal, and confers little discriminating power.

Rotational diffusion

Methyl group oscillations. Monte Carlo treatment at different temperatures reveals the actual mechanism of methyl oscillation–rotation in crystals. The total barrier includes an intramolecular term, calculated *ab initio* and incorporated in a torsional potential function, and intermolecular terms, deriving from the local environment at the rotating group. These latter terms may be revealed by inspection of radial distribution functions (RDFs).

The intramolecular barrier to methyl rotation in methylbenzene is almost null (0.2 kJ mol^{-1}), hence any localization of methyl hydrogens in aromatic systems must result from intermolecular factors. For 1,3-dimethylbenzene Fig. 9 shows almost complete localization at 100 K with peaks in the torsion angle distributions at the values found in the experimental crystal structure. The radial distribution functions show no features below 3 Å, so that the origin of the intermolecular blocking factor cannot be traced from that source. The block is anyway swept out at 300 K where rotation is free.

At 100 K, 1,4-methylethynylbenzene (AYOJED) shows a single although very broad peak in the distribution of methyl H-atom orientations, centered at 60° (Fig. S14, ESI†). Inspection of the crystal structure shows that one methyl atom points to a neighboring acetylene π-cloud; in fact the methyl H···C acetylene RDF shows a rather marked feature at 2.75 Å. This small orientational preference is swept away at 300 K where the plot of the distribution of methyl torsion angles is nearly flat, indicating free rotation.

In the simulation of *n*-alkane crystals only 1–2% of methyl groups appear to be reorienting even at room *T*, which is some 50–100 K above the melting points. The intramolecular barrier of 5 kJ mol^{-1} (or 2*RT* at 300 K) allows a libration of ±20° but seems high enough to prevent fast reorientations. Fig. 10 shows however a non-negligible population of reorientations of the entire molecule in the *n*-octane crystal; it is impossible to deconvolute the two rotations, methyl and full molecule, from a simple geometrical analysis such as ours, but it is known experimentally that long-chain alkanes behave as liquid crystals around their melting points, and our simulation clearly reproduces this fact. On the other hand, in the EXODAW crystal the same intramolecular barrier allows only about 20% of the groups reorienting even at 100 K. All considered, methyl rotation appears to be a widespread phenomenon in crystals not far from their melting point.

The intramolecular barrier for rotation of the N–CH_3 group of *N*-methylcinnamamide (MCINAM10) is rather substantial, 5 kJ mol^{-1}, the minimum being for a conformation in which the CH bond eclipses the C═O bond. In the simulations, the distribution of methyl group torsion angles at 100 K shows isolated peaks around the experimental value, which survive at 300 K (Fig. S15a, ESI†); accordingly, the X-ray determination at

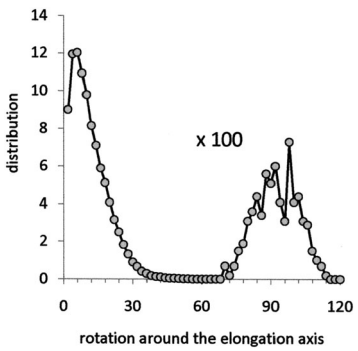

Fig. 10 Distribution of rotation angles around the elongation axis in the simulation of the *n*-octane crystal at 300 K. The rightmost part (>60°) has been magnified for clarity.

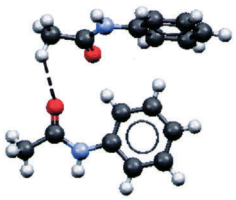

Fig. 11 The C–H···O feature in the X-ray crystal structure of acetanilide (C_6H_5–$NHCOCH_3$) determined at 113 K. Nitrogen: blue, oxygen: red.

room *T* shows ordered methyl groups. There are weak features in the RDF's for C–H···N and C–H···O=C distances of 2.8 and 3.2 Å, respectively, far larger than the sum of close contact radii. These broad signatures, that would hardly be qualified as C–H···X bonds, help the intramolecular barrier in preventing rotation.

The intramolecular barrier for methyl rotation in the (O=C)–CH_3 group of acetanilide (ACANIL01) is only 1.6 kJ mol^{-1}. The simulated distribution of methyl torsion angles at 100 K (Fig. S15b, ESI†) shows a peak for a staggered conformation, presumably favored by an intermolecular C–H···O contact preference (Fig. 11) witnessed by a broad peak in the corresponding CH···O RDF around 2.7 Å. Accordingly, the crystal structure appears ordered at 113 K. But at 300 K methyl rotation is predicted free by the simulation. One is tempted to conclude that unrecognizable C–H···X bonds seem effective in the first case, and recognizable C–H···X bonds seem ineffective in the second. The unavoidable message is that careful consideration is required before assigning bonding powers to any atom–atom short contact.

Dynamics of nitro groups. The simulations of nitro derivatives are only partly successful. Both aromatic (nitrobenzene, 1,4- and 1-3-dinitrobenzene) and aliphatic (JOHBUD, XOZBUK) show significant structural drifts from experiment, the most apparent being a general decrease in density, in the 7–13% range. Also peculiar is the variation in cell angles, by 10° in the monoclinic angle in 1,4-dinitrobenzene, and an almost unique (over our data sample) change of one orthorhombic angle from 90 to 104° in the 1,3-derivative. The reason for these partial malfunctions is hard to pinpoint; inspection of the RDF's is confusing. A reasonable guess is that the representation of Coulombic factors in "hard" nitro oxygens is particularly problematic.

The libration of nitro groups around the C–N axis is however well described: the intramolecular potential marks an energy cost of only 5 kJ mol^{-1} for a 45° oscillation, and the distribution of torsion angles in the simulations has peaks at zero degrees for nitrobenzene and at 5–11° for the dinitrobenzenes (Fig. S16, ESI†), in agreement with the observed crystal structures. Thus, the dihedral angle between the aromatic ring and the nitro group in these crystals is dictated by intermolecular factors.

Rigid-body molecular oscillation–rotation. In the benzene crystal, molecules are known to rotate in their plane even at low temperature.[28] A computational box of 192 molecules was set up using X-ray crystal cell dimensions at 15, 123, 218 K and (by extrapolation) at 273 and 300 K. NVT MC runs of 1 Mstep were then performed at each temperature. Fig. 12 shows the main result. At 15 K and 123 K the distribution of molecular

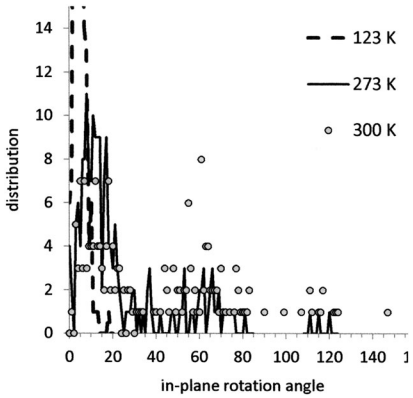

Fig. 12 Distribution of orientation angles in simulations of the benzene crystal at several temperatures.

oscillation angles is restricted to 10° or less. At 273 K the oscillation extends to 20°, and the simulation also catches a few molecules on the top of the barrier at 30° and 90°. At 300 K, formally above the melting temperature, the 0°, 60° and 120° wells are almost equi-populated and the rotational correlation function shows a marked decrease to 0.6. The simulated picture of molecular motion in this crystal is then quite satisfactory.

In-plane oscillations are more restricted for chlorobenzenes than for fluorobenzenes (Table 4); for l,4- and 1,2,4,5-fluorobenzenes, occasional 60° jumps are detected, while the 1,2,3-derivative seems prone to easy reorientation. The reasons for this difference are difficult to track, also recalling the partial malfunctions of fluorine potentials; the indication is however too clear to be overlooked. Note that room *T* is 30–50° higher than the melting temperatures of these derivatives. Translational diffusion functions in fluorobenzene crystals are larger than for other benzene derivatives, indicating a relative lack of internal cohesion, not unexpectedly.

A positive result is obtained for 1-chloroadamantane (BILNOZ01), which is a plastic crystal at room temperature: correspondingly, the distribution of orientation angles (Fig. 13) shows an extension up to 180° with a rotational correlation function drop to 0.5 over the 5 Mstep of the simulation. A longer simulation would probably have ended in a uniform distribution of orientation angles.

Table 4 Characteristics of the rotational diffusion in crystals of flat benzene derivatives in 5 Mstep runs at 300 K

Crystal	Range[a]	Jumps[b]	Transl. correl.[c]	Rotn. correl.[c]
Benzene	Continuous	~100; 7	0.76	0.844
Fluorobenzenes				
1,4	25	2; 0	1.4	0.967
1,2,4,5	20	0; 0	2.4	0.984
1,2,3	30	~80; 1	1.4	0.848
Chlorobenzenes				
Hexa	10	0; 0	0.25	0.995
1,2	16	1; 0	0.36	0.985
1,3,5	10	0; 0	0.55	0.995

[a] Range of rotation angles from zero. [b] Number of 60° and 120° jumps at the end of the simulation. [c] Values of the translational and rotational correlation functions at the end of the simulation.

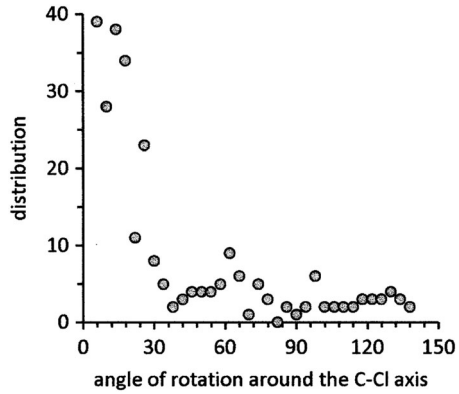

Fig. 13 Distribution of orientation angles about the axis of the C–Cl bond in chloroadamantane (BILNOZ01).

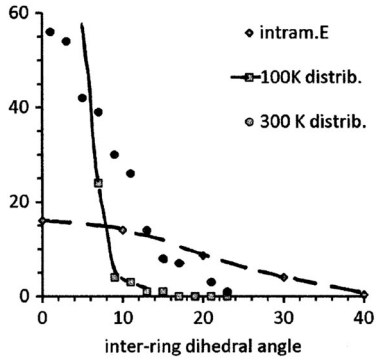

Fig. 14 Histogram of inter-ring torsion angles in simulations of the biphenyl crystal at 100 and 300 K. The dotted line is the intramolecular potential energy profile in kJ mol^{-1} units.

Inter-ring torsion. In molecules with two rings separated by a single bond there is usually competition between intramolecular factors, favoring a twisted conformation when steric impediments are at work, and intermolecular factors, generally favoring a planar conformation, better suited for efficient crystal packing. In the classical case of biphenyl (Fig. 14) the profile of intramolecular torsion potential energy has a minimum at 45°. For XAYMEP and ZIVKOE (see Scheme 1) the energy profile for inter-ring twist has a minimum at zero dihedral angle (planar structure) and is very shallow, with an expense of no more than 2.5 kJ mol^{-1} for an oscillation up to 40°. Yet the molecules are planar in the experimental crystal structures, and the distributions of torsion angles in the simulations peak at zero degrees with oscillation amplitudes of about 10–20°, in agreement with experiment.

Conclusions

A test of the atom–atom Coulomb–London–Pauli (AA-CLP) potential energy scheme in the Monte Carlo simulation of equilibrium structure and dynamics of organic crystals has been carried out over 63 crystal structures, a sample of unusual (unprecedented) width. The sample has compounds of widely varying chemical composition, hydrogen bonding or not, with rigid, semi-rigid and fully flexible molecular frames. The adequacy of the simulation is judged by comparison with experimental density, cell parameters, and when possible, sublimation enthalpies. Overall one sees here four cases of complete deviation, a few cases of substantial deviation, and a majority of acceptable or satisfactory results. Moreover, the simulated structure and energy changes on going from 100 K to room temperature are of the correct order of magnitude.

The equilibrium oscillations of methyl groups, of entire molecules in crystals of planar benzene derivatives, of linear-chain alkanes and in the plastic chloroadamantane crystal are well described. Cases of conformational competition between intra- and intermolecular factors, as in biphenyl, are simulated in agreement with experiment.

Weak directional preferences, like C–H···O interactions, can be sorted out through the use of radial density functions. Their role is somewhat toned down when, rather than just studying static atom–atom contacts, the dispersion of relevant contact distances is analyzed in a simulation of the oscillation around equilibrium values. In this and many other respects, this work demonstrates the much richer picture of crystal packing that can be obtained in dynamic simulations, as opposed to inspection of static crystal structures.

The force field and the set-up of the MC treatment provide an acceptable tool for the simulation of the properties of organic crystals in general. The emphasis on this work is rather on a broad-brush approach to a tool of general applicability, than on exhaustive optimization of a force field for a single molecule to reach many-digit agreement with experimental quantities; in this approach, running dynamic simulations does not require month-long efforts or the specialized experience. Monte Carlo has been preferred over Molecular Dynamics, perhaps more versatile in the treatment of molecular motion, for its simplicity, more immediate comprehensibility, and easier modification in view of future use in the simulation of phase transitions. The computer programs used here are available for free distribution to allow revision and duplication of the results. The only input required is basic crystallographic information, plus a reasonable amount of man-time and a more than affordable amount of computer time. The whole setup has its *forte* in the high ratio between quality of results and expense. Other computer program packages are available for the same task, so that a wider application of this kind of analysis is encouraged, as opposed to sometimes questionable speculation on static data from packing diagrams.

The atom–atom point-charge method has an intrinsic shortcoming in the representation of Coulombic contributions, due to the localization of atomic charges on nuclear positions. This approach is extremely simple and straightforward, but does not reproduce the substantial component due to penetration energy. Discrepancies appear in comparison with exact Coulombic energies provided by the fine-mesh integration of the PIXEL method. This problem is unavoidable and cannot be solved by improvement of the parameterization, but it is at least well understood, and it is mitigated by the fact that in many cases even a small overestimation of dispersion, or

underestimation of repulsion, provides a cancellation of errors. This defect is conspicuous for aliphatic hydrocarbons and for chlorine derivatives; moreover, for chlorine and other halogens, the distribution of intermolecular contacts is not spherical and interaction is anisotropic.[29] As before observed, we freely admit that other force fields may perform better than AA-CLP for single compounds or for some classes of compounds.

The appraisal and the refinement of the force field are certainly worthwhile tasks, but, in perspective, a more pressing goal is the use of the potential energy scheme and of the Monte Carlo procedure for the analysis of crystallization paths by the symmetry-bias method: results obtained[30] using the scheme in its present status already show some promise for the investigation of the twilight zone between the liquid and the crystalline state.

References

1 P. M. Agrawal, B. M. Rice, L. Zheng and D. L. Thompson, *J. Phys. Chem. B*, 2006, **110**, 26185–26188.
2 B. P. van Eijck, *Mol. Simul.*, 1994, **13**, 221–230.
3 A. Gavezzotti, *Chem.–Eur. J.*, 2000, **6**, 2288–2294.
4 A. Nemkevich, H.-B. Burgi, M. A. Spackman and B. Corry, *Phys. Chem. Chem. Phys.*, 2010, **12**, 14916–14929.
5 M. Tremayne, B. M. Kariuki and K. D. M. Harris, *Angew. Chem., Int. Ed. Engl.*, 1997, **36**, 770–772.
6 J. Kundin, C. Yurudu, J. Ulrich and H. Emmerich, *Eur. Phys. J. B*, 2009, **70**, 403–412.
7 L. A. Zepeda-Ruiz, A. Maiti, R. Gee, G. H. Gilmer and B. Weeks, *J. Cryst. Growth*, 2006, **291**, 461–467.
8 C. Chiccoli, P. Pasini, R. Texeira de Souza, L. R. Evangelista and C. Zannoni, *Phys. Rev. E: Stat., Nonlinear, Soft Matter Phys.*, 2011, **84**, 041705.
9 J. K. Brennan, B. M. Rice and M. Lisa, *J. Phys. Chem. C*, 2007, **111**, 365–373.
10 P. M. Agrawal, B. M. Rice, L. Zheng, G. F. Velardez and D. L. Thompson, *J. Phys. Chem. B*, 2006, **110**, 5721–5726.
11 A. Gavezzotti, *J. Am. Chem. Soc.*, 2000, **122**, 10724–10725.
12 A. Gavezzotti, *CrystEngComm*, 2011, **13**, 3573–3579.
13 J. Anwar, S. Tuble and J. Kendrick, *J. Am. Chem. Soc.*, 2007, **129**, 2542–2547.
14 J. Pillardy, Y. A. Arnautova, C. Czaplewski, K. D. Gibson and H. A. Scheraga, *Proc. Natl. Acad. Sci. U. S. A.*, 2001, **98**, 12351–12356.
15 M. A. Neumann, F. J. J. Leusen and J. Kendrick, *Angew. Chem., Int. Ed.*, 2008, **47**, 2427–2430.
16 R. Podeszwa, B. M. Rice and K. Szalewicz, *Phys. Chem. Chem. Phys.*, 2009, **11**, 5512–5518.
17 G. M. Day, *Crystallogr. Rev.*, 2011, **17**, 3–52.
18 S. L. Price, *Acc. Chem. Res.*, 2009, **42**, 117–126.
19 (*a*) P. Raiteri, R. Martonak and M. Parrinello, *Angew. Chem., Int. Ed.*, 2005, **44**, 3769–3773; (*b*) M. Salvalaglio, T. Vetter, F. Giberti, M. Mazzotti and M. Parrinello, *J. Am. Chem. Soc.*, 2012, **134**, 17221–17233.
20 A. Gavezzotti, *New J. Chem.*, 2011, **35**, 1360–1368.
21 F. H. Allen, *Acta Crystallogr., Sect. B: Struct. Sci.*, 2002, **58**, 380–388.
22 A. Gavezzotti, *CrystEngComm*, 2008, **10**, 389–398.
23 M. P. Allen and D. J. Tildesley, *Computer simulation of liquids*, Oxford University Press, Oxford, 1989, pp. 41 and 124.
24 A. Gavezzotti, *Mol. Phys.*, 2008, **106**, 1473–1485.
25 J. S. Chickos and W. E. Acree, *J. Phys. Chem. Ref. Data*, 2002, **31**, 537–698.
26 (*a*) A. Gavezzotti, *Molecular Aggregation*, Oxford University Press, Oxford, 2007, p. 276; (*b*) A. Gavezzotti, *Molecular Aggregation*, Oxford University Press, Oxford, 2007, ch. 7.
27 J. D. Dunitz, *ChemBioChem*, 2004, **5**, 614–621.
28 J. H. Ok, R. R. Vold, R. L. Vold and M. C. Etter, *J. Phys. Chem.*, 1989, **93**, 7618–7624 and references therein.
29 S. C. Nyburg and C. Faerman, *Acta Crystallogr., Sect. B: Struct. Sci.*, 1985, **41**, 274–279.
30 A. Gavezzotti, *CrystEngComm*, 2011, **13**, 3573–3579.